Swolfs Y., Pinho S.T., Composites Science and Technology 182 (2019) 107731
doi.org/10.1016/j.compscitech.2019.107731

# 3D printed continuous fibre-reinforced composites: bio-inspired microstructures for improving the translaminar fracture toughness

Yentl Swolfs*[1,2], Silvestre T. Pinho[2]

[1]Department of Materials Engineering, KU Leuven, Kasteelpark Arenberg 44 box 2450, Belgium
[2]Department of Aeronautics, Imperial College London, South Kensington Campus, SW7 2AZ, London, United Kingdom
*Corresponding author: Y. Swolfs (yentl.swolfs@kuleuven.be), Tel.: +3216373616

## Abstract

Translaminar fracture toughness is a vital property governing the notch sensitivity and damage tolerance of composites. Nature has shown that incorporating material transitions can increase toughness significantly. This work presents finite element models demonstrating that such transitions can indeed increase the translaminar fracture toughness. The designed microstructures were then 3D printed using continuous glass and carbon fibres. The specimens consisted primarily of glass fibres, but with local carbon fibre strips. A new compact tension specimen with a side groove was designed to ensure proper failure. When the strips were sufficiently large, toughness improvements of 20-60% were found after the crack had grown through the strips. These results reveal a powerful strategy for locally increasing the toughness in areas where it is needed the most.

**Keywords:** A. Hybrid composites; A. Polymer-matrix composites (PMCs); B. Fracture toughness; B. Synergism;

## 1 Introduction

Fibre-reinforced composites offer high stiffness and strength for a low density, making them a common material in lightweight applications. They are, however, also limited by their inherent brittleness and sensitivity to damage. The industry is therefore moving towards more damage-tolerant designs. This requires being able to reliably measure, predict and optimise the toughness of composites, which remains a significant challenge [1].

In homogeneous, isotropic materials, the fracture toughness is the same in all directions. In composites however, three distinct types of fracture toughness exist: interlaminar, intralaminar and translaminar [1,2]. Interlaminar implies a crack in between the plies whereas intralaminar implies a crack inside the plies. In both cases, however, fibre fractures are not required for the crack to propagate. In translaminar fracture, the cracks grows perpendicular to the fibres, thereby fracturing fibres and eventually the entire ply. The translaminar fracture toughness governs the damage tolerance and notch sensitivity of composite materials [1-4].

The compact tension test has established itself as the most widely used test for measuring the translaminar fracture toughness in tension. The reported values for 0° carbon fibre/epoxy plies are in the range of 20-280 kJ/m² [1,3-7]. This is significantly higher than interlaminar fracture toughness values, which typically range from 0.2 to 3 kJ/m² [7-11]. This is primarily because translaminar fracture is controlled by significant fibre/matrix debonding and pull-out, both of which can absorb large amounts of energy.

When looking for strategies to improve toughness, it is useful to draw inspiration from materials with a unique stiffness-toughness combination [12,13]. Nature offers several examples, and the microstructure of nacre in particular inspired many researchers [14-16]. While the mechanisms contributing to the surprisingly high toughness of nacre are complex, its alternation of soft and hard phase is certainly an important contributor. Kolednik et al. [16] therefore explored whether the material transitions within nacre can contribute to increasing toughness. They proved that the strain energy release rate lowers when the crack grows into a compliant layer. When this rate is lower than the critical value, the crack cannot grow anymore until the external forces are increased. Several follow-up studies confirmed that material transitions are therefore an efficient strategy for crack arrest [17-19].

Another approach to increasing the toughness of composite materials is to exploit fibre-hybridisation [2,20]. This has often led to synergetic effects, where the fibre-hybrid composites offered a toughness above the value expected from rules-of-mixtures based on the constituent non-hybrid composites. Synergetic effects have been reported for a range of toughness-related parameters, such as open-hole tensile strength [11,21], penetration impact resistance [22] and translaminar fracture toughness [6,22]. Fibre-hybridisation also inherently offers variations in material properties, thereby exploiting bio-inspired toughening concepts [16-19]. The challenge, however, is that the microstructure should vary along the crack growth direction. In interlayer fibre-hybrid composites, which is the most common configuration [20], the material properties vary along the thickness, but not within the plies. In finely dispersed intrayarn hybrids, the alternating material properties will likely be at a too small scale to trigger some desirable toughening mechanisms. Intralayer hybrids therefore seem like the most suitable hybrid configuration, although they are more complicated to manufacture than interlayer hybrids.

The material transitions concept of Kolednik et al. [16] was also developed separately by researchers in the field of composite materials [23-25]. The initial strategy involved adding external strips of a different material to the base laminate [23], turning it into an interlayer hybrid configuration. Later studies integrated 7-13 mm wide strips into the laminate itself [24], hence creating an intralayer hybrid configuration. Their notched tensile tests did show an increased failure strain when strips were added, but they did not directly analyse fracture toughness.

Conventional manufacturing approaches would struggle to create optimal microstructures with material transitions. This is one of the many reasons why 3D printing of fibre-reinforced composites has grown so strongly in the last decade [26]. There is some discussion on the suitability of the terminology, as some authors argue that 2.5D printing is more appropriate [27]. Here, the term 3D printing will be used, as it has been the prevailing terminology in the literature [26,28]. We propose to demonstrate for the first time in the literature the potential of 3D printing for mass-produced and bespoke hybrid composites with locally-tailored toughness. We will achieve this by exploiting the design freedom of 3D printing to manufacture intralayer hybrid composites where the crack grows through alternating carbon/glass layers. A finite element model is developed to identify a suitable microstructure, and compact tension tests are performed to confirm the conceptual ideas revealed by the modelling predictions.

# 2 Finite element model for translaminar fracture

## 2.1 Model setup

A finite element model of a compact tension test was developed in Abaqus/Explicit 6.14. A rectangular specimen geometry was used with a length of 65 mm and a height of 60 mm. The carbon and glass fibre composite materials were assumed to be linearly elastic with their engineering constants based on the engineering constants for unidirectional plies described in Table 1. Classical laminate theory was used to convert these values to engineering constants for a balanced cross-ply laminate. The majority of the specimen was modelled using shell elements, whereas the fracturing region was modelled using 3D solid elements (see Figure 1a). The fracturing region was modelled using cohesive zones, with the cohesive laws presented in Figure 1b. The cohesive strength and fracture toughness are realistic values for the respective cross-ply laminates they represent [1,6,22]. Cohesive elements were placed in between material transitions, which are hence on a plane perpendicular to the fracturing region (see Figure 1a). These elements were only 10 μm thick and were not allowed to fail. They were only used to prevent cohesive zones of two different materials from sharing nodes, and hence serve as mere tie constraints. The load was applied as two point loads with a smooth ramp-up to avoid introducing artificial stress waves.

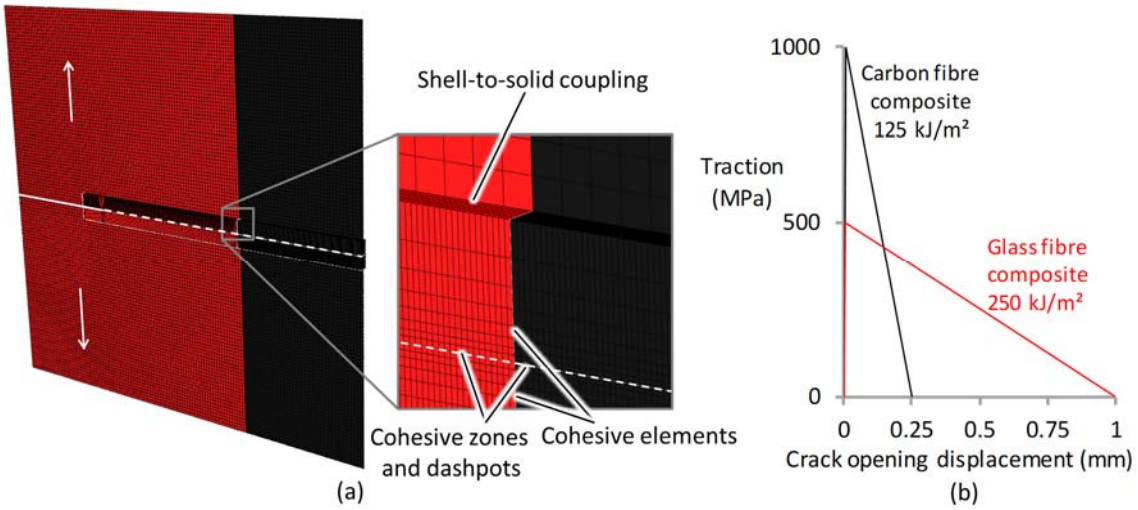


**Figure 1: The finite element model for translaminar fracture: (a) 3D view with the arrows indicating the loading points and (b) the cohesive laws used for the carbon and glass fibre composites. The full white line indicates the initial crack and the dashed white line the fracturing region. The dashpots are not shown.**

Due to the large energy release during translaminar fracture, crack growth tends to create significant force oscillations in the model. To counteract this, the crack surfaces were connected with viscous dashpots. These dashpots were more viscous near the initial notch tip, as this region had to deal with the largest energy releases. The viscous energy dissipation in the model was carefully monitored and its increase was limited to reasonable levels. Further reductions in this viscous energy increase yielded nearly the same toughness and force-displacement diagrams. A mass scaling factor of 40 was applied to the cohesive elements only, as they are the smallest elements and hence limit the stable time increments. This scaling sped up the simulations, while keeping the kinetic energy at less than 1% of the strain energy for most of the time. The highest kinetic/strain energy ratio was detected for the GF-CF and GF-CF-GF models, where this reached 15% and 10% respectively. This ratio, however, occurred after the crack propagated past the

material transition or strip, and is hence in a region that does not affect the conclusions drawn later on.

Figure 2 presents the three pairs of models that were created and analysed. The first pair consists of the pure glass fibre (GF) and pure carbon fibre (CF) reference composite (see Figure 2a and d). In the second pair of models, the cracks have to grow through a material interface: a GF-CF transition (see Figure 2b) or a CF-GF transition (see Figure 2e). The final pair of models has a 2 mm wide strip where the material is different from the rest of the model. This includes a GF strip inside a CF composite (see Figure 2c) and a CF strip inside a GF composite (see Figure 2f).

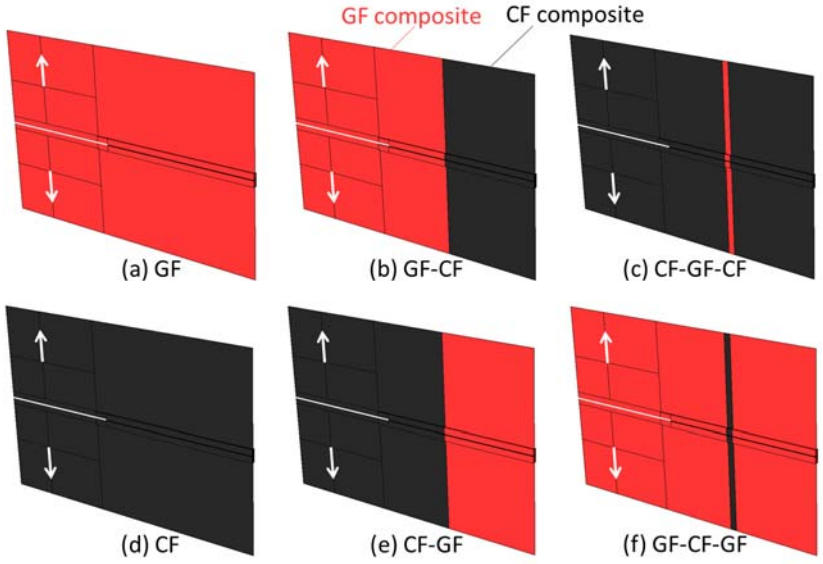


**Figure 2: Six finite element models with no or with different material transitions: (a) GF, (b) GF-CF, (c) CF-GF-CF, (d) CF, (e) CF-GF, and (f) GF-CF-GF. The initial crack is indicated with a white line, with the crack growing from the left- to the right-hand side.**

The local crack extension was defined as the initial point in the cohesive region (i.e. where traction is maximum and damage is minimum). The local crack extensions were averaged out over the thickness, as the crack front was slightly curved. This approach corresponds well with the experimental crack length observations, which is based on visual identification of crack tip openings. The fracture toughness of the models was calculated by extracting the traction and crack opening displacement of all the nodes in the process zone. The area underneath this traction-displacement diagram was then integrated to obtain the translaminar fracture toughness of the model as a whole for that given crack length or time. This extraction method was successfully validated against the traditional approach based on the compliance change equation (see equation 1 in section "3.2 Compact tension tests"). The latter approach yielded similar results for the hybrid specimens but with significantly more scatter, and was hence not used in the final results.

## 2.2 Model predictions

Figure 3 presents the force-displacement diagrams predicted by the finite element models. The GF and CF reference models have the expected response, with a slightly more stable behaviour for the GF reference. The GF-CF and GF-CF-GF models reveal a higher force required for a given displacement than the GF reference model. This proves that material transitions can cause crack arrest.

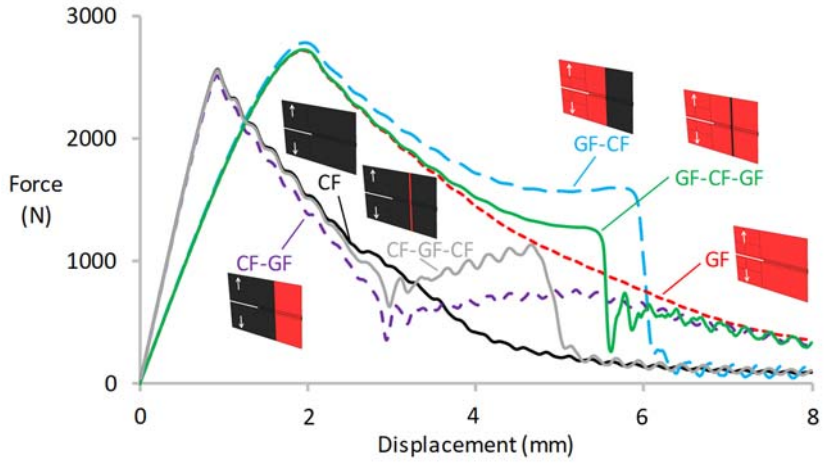


**Figure 3: Force-displacement diagrams of six different finite element models.**

The interesting behaviour of the GF-CF and GF-CF-GF models is confirmed in the fracture toughness evolutions in Figure 4. This figure proves that crack growth through a material transition increases the toughness. This creates a material that locally has a higher fracture toughness than either of the constituent composites. The small dip of GF-CF-GF after its maximum toughness reveals the locally increased toughness is followed by a local decrease of the toughness. In the CF-GF and CF-GF-CF models, this dip comes before the increase. This shows that crack growth from CF into GF negatively affects the toughness, whereas the other way around enhances toughness.

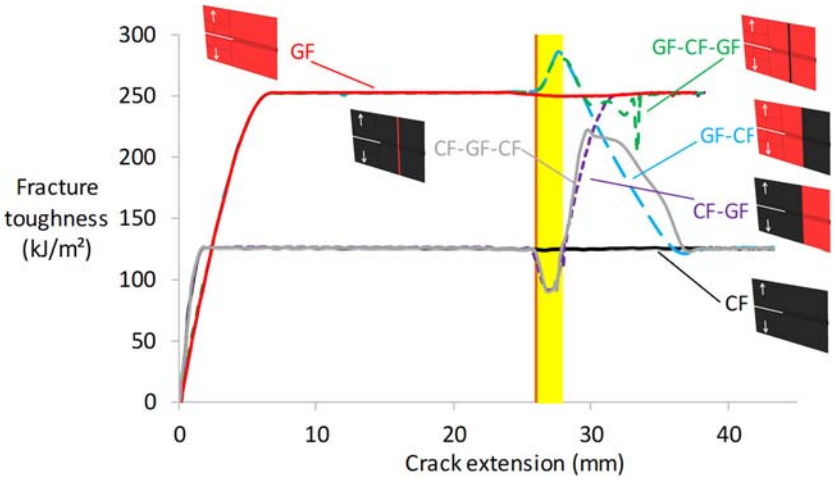


**Figure 4: Fracture toughness evolution of the six different finite element models as a function of crack extension. The vertical orange line indicates the start of the material transition in the GF-CF and CF-GF models, whereas the yellow region indicates the width of the strips in GF-CF-GF and CF-GF-CF models.**

Two additional models were run to identify the origin of the synergies. Both models were based on the GF-CF model with slight alterations to the CF region. In the first model, the cohesive laws were the same as in the GF-CF model, but the GF engineering constants were applied to the CF region. In the second model, the engineering constants were the same as in the GF-CF model, but the GF cohesive law was applied to the CF region. The synergetic effect reached 286.7 kJ/m² for the first model, compared to 285.1 kJ/m² for the

GF-CF reference model. For the second model, the synergetic effect disappeared. This proves that the synergy is caused by the difference in cohesive laws and hence translaminar fracture behavior of the GF and CF regions and that the stiffness difference does not affect this synergy.

Figure 5 plots the traction-separation law that was identified at the peak fracture toughness value for the GF-CF model in Figure 4. The toughness value at this point was 285.1 kJ/m², which is well above the toughness values for the constituent CF and GF materials. Figure 5 provides further evidence of the origin of the synergy being the difference in translaminar fracture behavior of the GF and CF regions. This allows the material to sum up contributions of both cohesive laws, allowing the area underneath the traction-separation law to rise significantly higher than 250 kJ/m². In practice, this phenomenon is related to the pull-out lengths. The cohesive laws that were used (see Figure 1b) imply that the carbon fibre has shorter pull-out lengths than glass fibre, as seen from its smaller maximum crack opening displacement. The hybrid therefore has a specific crack extension for which relatively CF pull-outs contribute significant toughness at small crack opening displacements while at the same time still benefiting from the longer GF pull-outs that lie further behind the crack tip (see Figure 5). This creates guidelines into what type of fibre-reinforced composites to combine if their traction-separation laws are known.

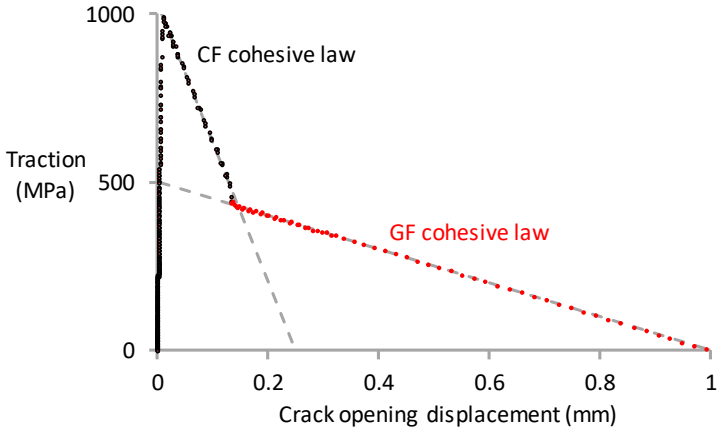


**Figure 5: Traction-separation law identified at the peak fracture toughness value for the GF-CF model.**

# 3 Materials and methods

## *3.1 Materials and 3D printing*

The specimens were printed using a MarkOne 3D printer from MarkForged. This printer has two nozzles: one nozzle prints unreinforced nylon polymer, whereas the other one prints continuous fibre-reinforced nylon. The default nylon, carbon/nylon and glass/nylon filaments from the manufacturer were used. The fibre volume fraction of the carbon/nylon and glass/nylon filaments were measured to be 32% and 33%, respectively, based on matrix burn-off tests. Each layer was 100 μm thick, with the only exception being the 0° block for the carbon fibre reference composites.

The compact tension test requires 0° and 90° plies to bear the loads and avoid undesired failure modes. The MarkOne 3D printer is not naturally capable of printing hybrid composites. We therefore developed an original procedure to enable this by splitting the printing procedure into three steps. In the first step, a part of 210x90x5 mm was printed using the glass fibre settings (see Figure 6a). This part was printed with as many fibre

layers as possible. The isotropic fibre fill option was used, implying that all fibres were oriented in the length direction (210 mm) of the part. To maximise the fibre content, the print used the minimum nylon requirements imposed by the software: one wall, one floor and one roof layer. The software allows printing alternating 0° and 90° plies, but does not allow the incorporation of alternating glass and carbon fibres within the same ply. For the hybrid composites, all layers were printed using the glass fibre settings. The carbon fibre layers were included by pausing the print and temporarily replacing the spools. The first two configurations had a 2 mm and a 6 mm carbon fibre strip respectively. The third configuration had three 1 mm carbon fibre strips separated from each other by 1 mm glass fibre strips. This configuration will be referred to as 5 mm alternating strip specimens. These strips are smaller than the 7-13 mm wide ones used by Poe and Kennedy [24], and could easily be downscaled down to 100 µm. Although the present specimens could potentially be manufactured using conventional composite processes, it would be tedious and difficult to achieve a sharp material transition. For downscaling to 100 µm strips, 3D printing is the only viable solution.

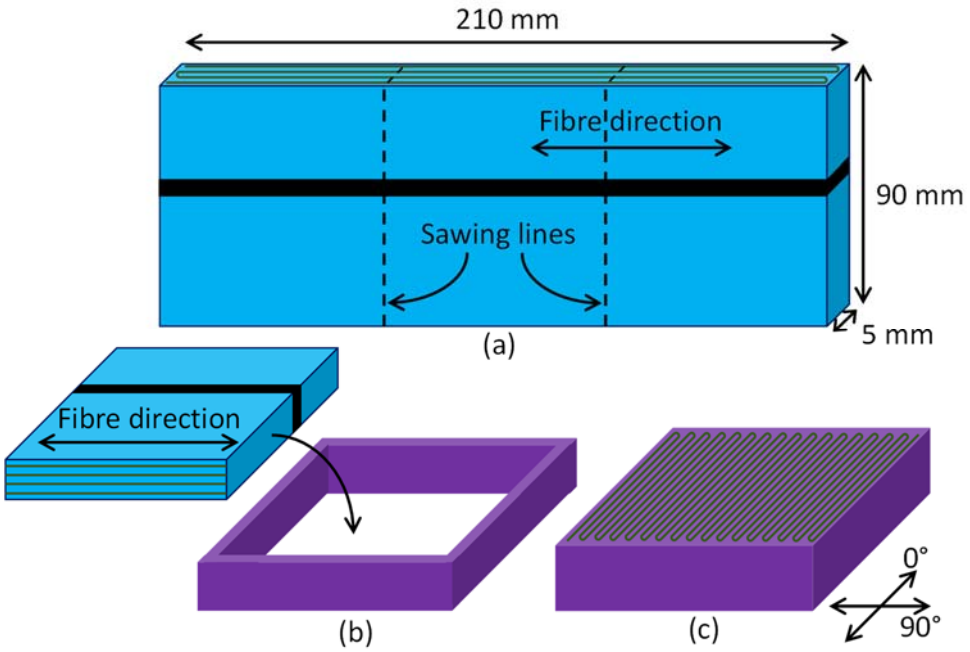


**Figure 6: Schematic overview of the first two printing steps: (a) printing of the middle 0° block, (b) printing the first half of one 90° block to insert a 0° block, and (c) printing the second half of one 90° block by overprinting of the 0° block.**

The complete part was then sawed in three parts along the dashed lines in Figure 6a, using a circular saw. The second step printed a rectangular box with an open bottom (see Figure 6b and c). This part is approximately 72x92x6 mm with upright walls approximately 1 mm thick and consisting of pure nylon. Before printing the roof of this box, however, the print was paused and one of the 70x90x5 mm specimens from step 1 was inserted into the open box (see Figure 6b). The print was then resumed, after which two nylon layers, 8 glass fibre layers and again 1 nylon layer were overprinted on the inserted specimen (see Figure 6c). The fibre layers printed in step 2 were all in the same direction, and perpendicular to the layers printed in step 1.

The third step is essentially a repetition of the second step, with the specimen now flipped 180° to print layers on the other side. This results in a 90°/0°/90° layup, with glass fibres only in the 90° layers, and glass or glass/carbon fibres in the 0° layers (see Figure 7).

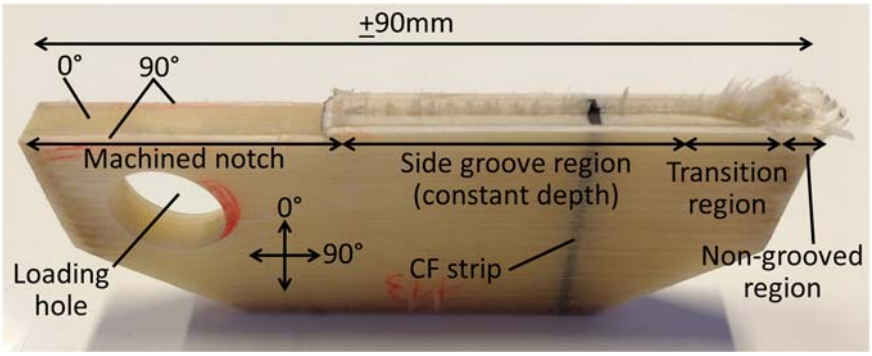


**Figure 7: Half of a fractured compact tension specimen, showing the layup, the location of the strip, the machined notch and the side groove. The scale bar is only approximate due to the 3D nature of the photograph.**

## 3.2 Compact tension tests

After printing, the specimens were rectangular with nominal dimensions of 74x94x7 mm. The specimen perimeter, the loading holes and part of the notch were then water jet cut to the double tapered shape recommended by Blanco et al. [29]. The shape of the initial crack was refined using a circular saw with a thickness of 3 mm and sharp tip. The initial crack length was 30 mm, measured relative to the centre of the loading holes. The notch was finally sharpened using a sharp blade, as recommended by Laffan et al. [30]. Finally, a side groove was machined into the specimens using a circular saw with a thickness of 1 mm and a diameter of 50 mm (see Figure 7). The remaining average thickness inside the groove ranged between 330 and 940 μm depending on the specimen. The last 5 mm of the specimens were left at full thickness to ensure it could withstand the compressive stresses (see Figure 7). The side groove is vital in preventing compressive failure at the back of the specimen, which is caused by a combination of the high translaminar fracture toughness and low compressive strength of the 3D printed materials.

Compact tension tests were performed on an Instron 5969 with a 50 kN load cell and an Instron 5567 with a 30 kN load cell. The loading rig and pins had the same design in both cases. Preliminary tests (not detailed here) revealed that the specimens were prone to buckling before fracture initiation. To prevent buckling, a steel anti-buckling guide was clamped on the top and bottom of the specimen using four screws that were loosely tightened by hand. This guide was sufficient to prevent buckling without interfering with the test results. This was confirmed by interrupting a test, removing the guide near failure initiation, and confirming that this did not noticeably change the load.

If the engineering constants of the plies and the geometry of the specimen are known, then linear elastic finite element models can be used to determine the crack length for a given load [1]. In the present case, these models also need to include the precise geometry of the side groove and the exact position and material properties of the strips to yield reliable results. Table 1 summarises the engineering constants used in the compliance calibration model. The $E_{11}$ values were obtained from tensile tests. The Poisson's ratio for the matrix was estimated from the literature. The carbon fibre engineering constants in Swolfs et al. [31] were then used in conjunction with the measured fibre volume fractions and the Chamis' micromechanical formulae [32] to obtain the rest of the values.

**Table 1: Engineering constants of the unidirectional plies that were used in the finite element model for compliance calibration.**

| | Nylon | Carbon fibre/nylon | Glass fibre/nylon |
|---|---|---|---|
| $E_{11}$ (GPa) | 0.45 | 73.9 | 26.70 |
| $E_{22}$ (GPa) | 0.45 | 1.00 | 1.05 |
| $G_{12}$ (GPa) | 0.16 | 0.37 | 0.38 |
| $G_{23}$ (GPa) | 0.16 | 0.36 | 0.38 |
| $\nu_{12}$ (-) | 0.40 | 0.35 | 0.34 |

Despite basing these engineering constants on measurements, they still resulted in an underprediction of the compliance *C*. This is likely due to the void content and the local deformation around the loading holes, both of which were ignored. The entire numerical compliance curve *C(a)* was therefore shifted vertically upwards by the experimental/numerical compliance ratio before the onset of non-linearity, at which point the crack length is accurately known. For every measured crack length, the corresponding, corrected numerical compliance was used in the data reduction. Note that this approach eliminates the contribution of plasticity to the energy dissipation, which was a desired outcome. The strain energy release rate was then calculated as:

$$\frac{F^2}{2t}.\frac{dC}{da}, \tag{1}$$

where *F* is the applied load, *t* the thickness inside the side groove and *dC/da* the slope of the compliance *C* as a function of the crack length *a*.

The last part of the crack extension was removed from all results to prevent interference with the end of the side groove. The strain energy release rate was normalised to the thickness *t* of the fractured material, and not to the width of the entire specimen (see equation 1). Figures will present the strain energy release rates, with the critical values marked by an 'x'. These values correspond to the translaminar fracture toughness. The force-displacement diagrams show the force divided by thickness of the fracturing material inside the side groove. This normalisation helps to reduce the scatter introduced by variations in the thickness of fracturing material.

### *3.3 Scanning electron microscopy*

Scanning electron microscopy was performed on Hitachi S-3700N and Philips XL30-FEG machines to perform fractography, and measure the width of fractured material. The applied voltage was 10 kV. The specimens were coated with a thin layer of gold or platina to ensure good conductivity and inhibit specimen charging. Scanning electron microscopy was used to analyse the fracture surface, and to measure the thickness of the fractured material.

## 4 Experimental results

The modelling predictions revealed significant potential improvements in the translaminar fracture toughness. The most promising configuration were strips of carbon fibre inside a glass fibre composite. The experiments therefore focused on glass fibre specimens with carbon fibre strips.

### *4.1 Reference specimens*

Figure 8 plots the results for the compact tension tests on six glass fibre and four carbon fibre composites. The glass fibre composites displayed more stable crack growth with

smaller crack jumps and load drops (see Figure 8a) than the carbon fibre composites (see Figure 8). Significant scatter is present, which is partially due to the significant material variations common in 3D printing [33,34]. A second reason is that the thickness varies by 20-30% inside the groove, but the calculations used the average thickness. A closely related issue is that the translaminar fracture toughness increases with ply thickness [4,7].

The initiation toughness values were 126 ± 48 kJ/m² and 103 ± 31 kJ/m² for glass and carbon fibre composites, respectively. When the first 5 mm crack extension are discarded, the average propagation toughness was 197 ± 61 kJ/m² for the glass fibre composites. Steady-state propagation was not achieved for the carbon fibre composites, but it is clear that the propagation toughness is higher than that of the glass fibre composites.

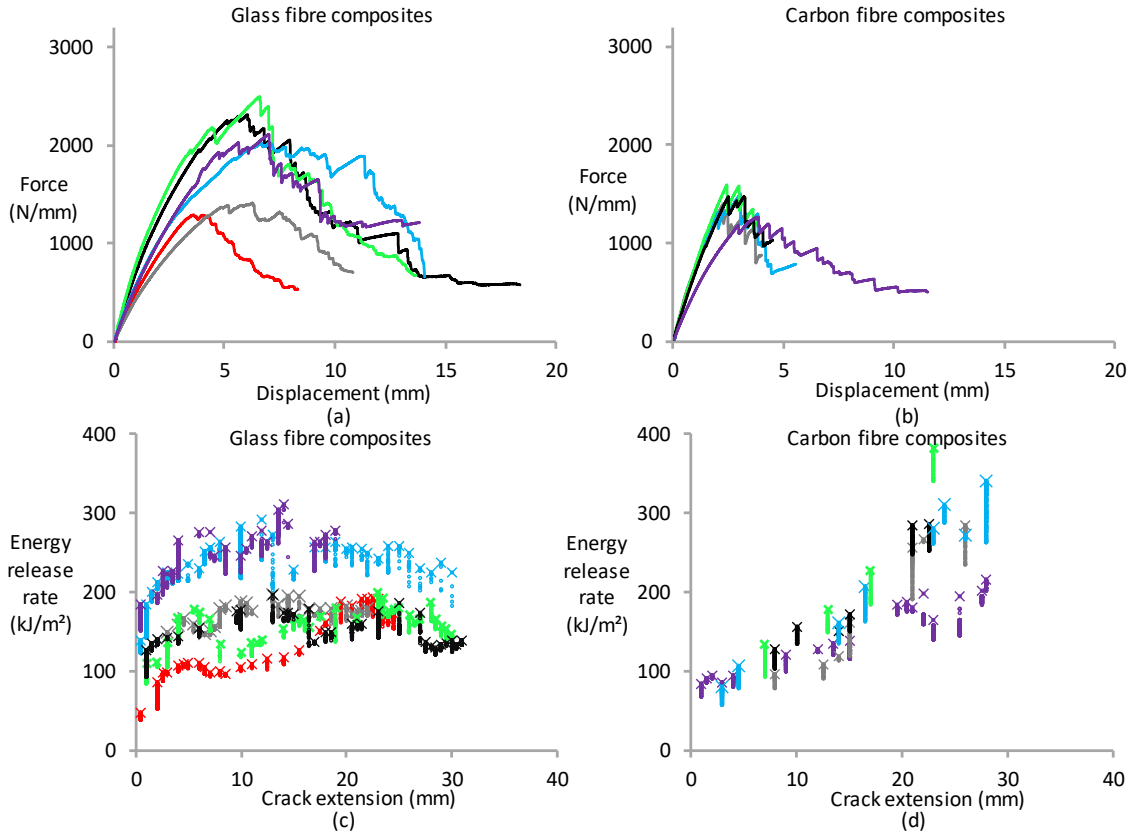


**Figure 8: Results of the compact tension tests on reference composites: (a) force-displacement diagrams for the glass fibre composites, (b) force-displacement diagrams for the carbon fibre composites, (c) R-curves for the glass fibre composites, and (d) R-curves for the carbon fibre composites. The colours represent the matching specimens on the force-displacement diagram and R-curve. The energy release rate is plotted as a function of the crack extension, with 'x' indicating the critical values.**

The glass fibre composites show a slight, but consistent increase in the first 5 mm of crack extension (see Figure 8c), while the remainder of the R-curve is relatively flat. This is different for the carbon fibre composites, which display an increasing trend over the entire R-curve (see Figure 8d). This is attributed to a combination of the long pull-outs and the differences in material stiffness. The carbon fibre pull-outs were 2-5 mm (see Figure 9b), where the higher end of the range is close to the crack opening displacement at the end of the test. More pull-outs are hence being engaged as the specimen is being loaded further, and hence the toughness keeps increasing. For glass fibre however, the pull-out lengths were 1-4 mm (see Figure 9a) compared to crack opening displacements of about 10 mm

at the end of the test. Note that these pull-outs are significantly longer than those typically reported in the literature [3,7,22].

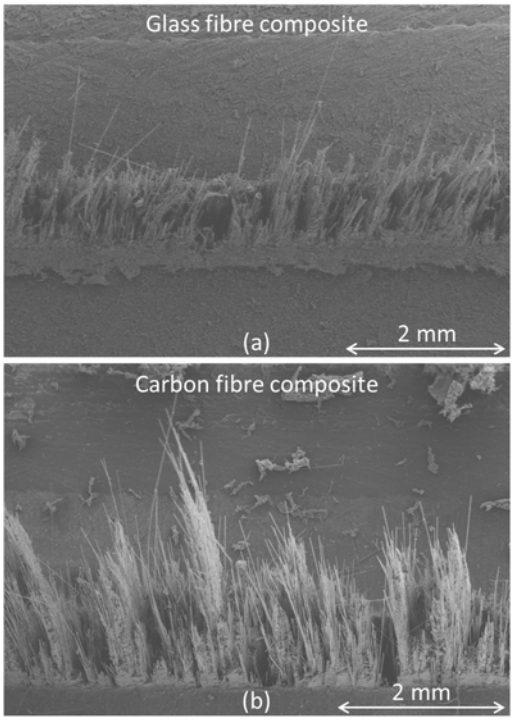


**Figure 9: Scanning electron microscopy images of the fibre pull-outs in a (a) glass fibre composite specimen and (b) carbon fibre composite specimen.**

## 4.2 2 mm carbon fibre strip specimens

Figure 10 presents the results for specimens with a 2 mm carbon fibre strip. The force-displacement diagrams show that the load drop near the carbon fibre strip seems to be preceded by a plateau-like region for some specimens (see Figure 10a). This indicates that the presence of the strip temporarily arrests crack growth. Some specimens reveal an increase in fracture toughness right after the strip (see Figure 10a), as predicted by the model (see Figure 4). The scatter in the data, which was also present in the reference composites, however, makes it difficult to consider this conclusive evidence.

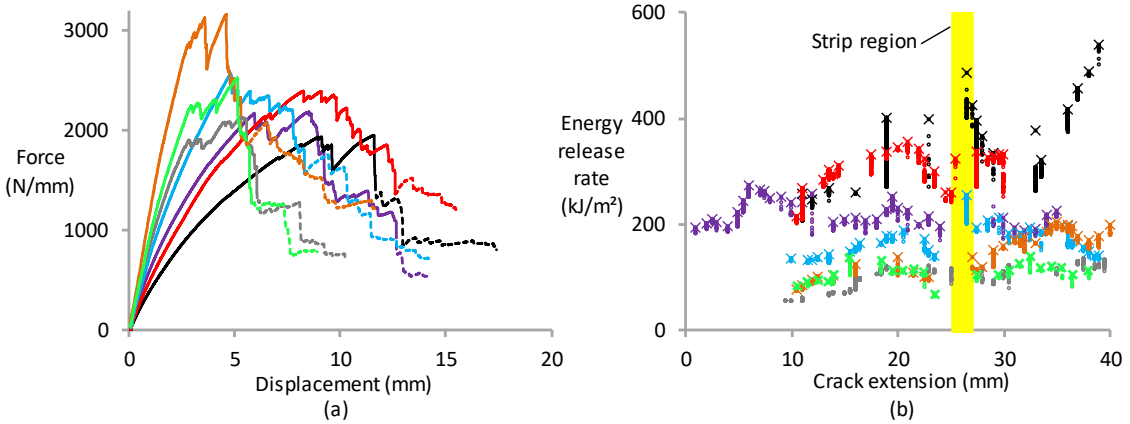


**Figure 10: Results of the compact tension tests on 2 mm carbon fibre strip specimens: (a) force-displacement diagrams, and (d) R-curves. The colours represent the matching specimens on the force-displacement diagram and R-curve. The dashed force-displacement curves represent the part after the crack has grown through the strip. The energy release rate is plotted as a function of the crack extension, with 'x' indicating the critical values. The crack extension values were shifted horizontally so that all strip regions coincide.**

## 4.3 6 mm carbon fibre strip specimens

The 2 mm carbon fibre strip specimens revealed some potential toughness increases, but they were not easy to detect due to the scatter in the data. The strip thickness was therefore increased from 2 to 6 mm in an attempt to find more pronounced effects. Figure 11 plots the results for 6 mm carbon fibre strip specimens. The results are now clearer: when approaching the strip, the crack growth is arrested (see Figure 11a), resulting in a plateau, similar to the model predictions for GF-CF-GF (see Figure 3). This crack arrest also results in a local increase in the fracture toughness (see Figure 11b). This increase was about 20-50%, depending on the exact data points that are considered for this calculation (see Figure 11b).

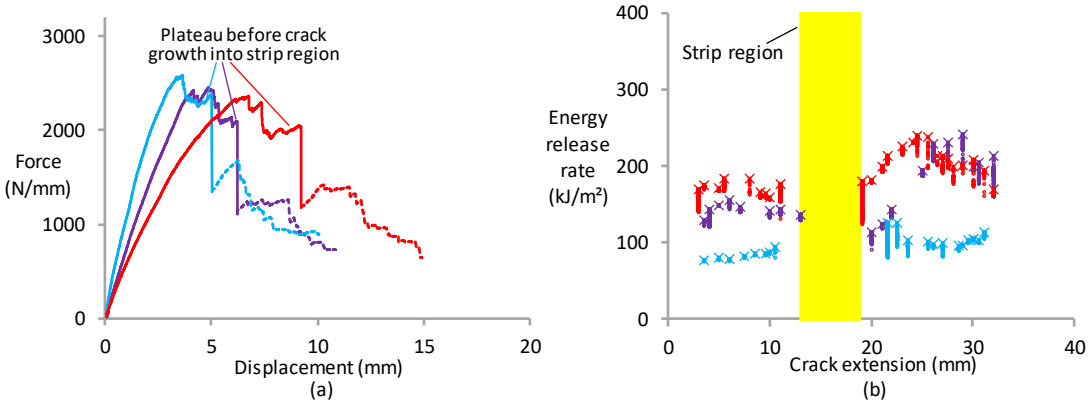


**Figure 11: Results of the compact tension tests on 6 mm carbon fibre strip specimens: (a) force-displacement diagrams, and (b) R-curves. The colours represent the matching specimens on the force-displacement diagram and R-curve. The dashed force-displacement curves represent the part after the crack has grown through the strip. The energy release rate is plotted as a function of the crack extension, with 'x' indicating the critical values. The crack extension values were shifted horizontally so that all strip regions coincide.**

## 4.4 5 mm alternating strip specimens

Another approach is to have an alternating strip of carbon-glass. This approach has the characteristic that it can potentially be applied all over the specimen rather than only locally. As a proof of concept, the strip here was composed of carbon-glass-carbon-glass-carbon strips of 1 mm each. The green and black curve in Figure 12a reveal a small plateau prior to growing through the strip. After the strip, they display an increase in fracture toughness of 43% and 61% respectively. This plateau in the force-displacement diagram is absent for the blue specimen, and the peak occurs at much higher values. Its toughness does show similar increases as the other specimens, although it is more challenging to quantify objectively.

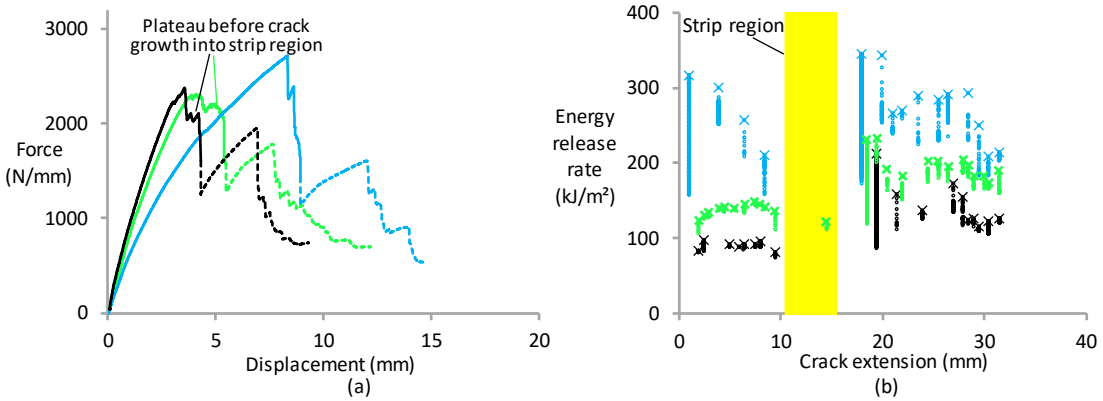


**Figure 12: Results of the compact tension tests on 5 mm alternating strip specimens: (a) force-displacement diagrams, and (b) R-curves. The colours represent the matching specimens on the force-displacement diagram and R-curve. The dashed force-displacement curves represent the part after the crack has grown through the strip. The energy release rate is plotted as a function of the crack extension, with 'x' indicating the critical values. The crack extension values were shifted horizontally so that all strip regions coincide.**

# 5 Discussion

The models predicted a local increase in the fracture toughness when a strip is reached, followed by a dip (see Figure 3). In the experiments, this increase was clearly observed for the larger strips, but the dip was often not clearly present. The absence of the dip may be linked to the long pull-out lengths relative to the crack opening displacement (see Figure 9b). This creates a long process zone length, allowing the effect of the strips to persist over a significant range of crack lengths. This could explain why the predicted dip is not observed in the R-curve.

The measured pull-out lengths inside the 2 and 6 mm carbon fibre strips were only 1-2 mm, which is significantly shorter than the 2-5 mm found in the full-carbon fibre reference composites. Increased pull-out lengths would have been one way to explain the observed synergetic effects, but that argument clearly cannot be used here. Kolednik et al. [16] revealed that the varying material properties can be enough to create crack arrest. Their arguments did not require changes in pull-out lengths, as their two material types did not contain any fibres.

Previous literature data found some synergetic effects for translaminar fracture toughness in tension [22] or none at all [6]. These effects were up to 15% higher than the linear rule-of-mixtures [22], whereas the experimental synergies reported here were significantly higher (20-60%). In the modelling predictions in particular (see Figure 4), the reported values were locally above the toughness of either of the two constituent materials. Incorporating material transitions can therefore yield truly synergetic effects for the translaminar fracture toughness. The strip-based approach seems to be a more promising strategy than the interlayer hybridisation strategy used elsewhere [22].

The reported propagation values were up to 540 kJ/m² (see Figure 10b), which is much higher than carbon/epoxy and glass/epoxy data in the literature [1,3-7,35]. This is in line with the pull-outs being significantly longer than lengths reported in the literature. It also highlights the benefit of the developed test method with the side groove, as it allows thick plies to be tested without any undesired failure mechanisms. This is the key reason why the literature has not been able to report higher values, as the regular compact tension test would lead to undesired failure mechanisms for such high toughness values [7].

The new specimen design offers significant potential: it allows to overcome the common difficulties in compact tension testing of materials that are either weak in compression, or have a high translaminar fracture toughness. For tougher or compressively weaker materials, the side groove can be machined deeper. A deeper groove leaves less material to fracture, which decreases the load required for crack growth and makes compressive failure less likely. This new specimen design, however, also has two significant drawbacks. Firstly, the design is susceptible to increased variations, both from specimen to specimen and within a specimen. Both variations are primarily due to inevitable variations in the groove depth, in combination with the thickness dependence of translaminar fracture toughness [7]. This implies that the variation of groove depth is not just a geometric effect that is taken into account by the thickness t in equation 1. This was an issue in the presented test results, even when the side grooves were machined using a computer-controlled device. Secondly, the groove can make it more difficult to observe crack growth. It should therefore be manufactured with a sufficiently thick blade, so that the groove is sufficiently open to monitor the crack length.

# 6 Conclusion

The finite element models confirmed that material transitions can locally increase the translaminar fracture toughness of composites. This allowed a true synergetic effect: the toughness of the fibre-hybrid composite was increased above the toughness of both composites. This effect was successfully confirmed using a new compact tension specimen design with a side groove. The experiments for 2 mm carbon fibre strips inside a glass fibre composite were not conclusive. For 6 mm carbon fibre strips and 5 mm alternating strips, a significant increase in translaminar fracture toughness was found right after the strip location. This proves that incorporating material transitions is a potent strategy for increasing the translaminar fracture toughness.

The proposed strategy can be useful for locally increasing the toughness in areas where stress concentrations or impact events are expected to happen. It demonstrates for the first time the potential of 3D printing for bespoke fibre-hybrid composites with locally tailored toughness. This could have a significant impact on the industrial implementation of locally toughened composites. Future research should focus on the development of dedicated 3D printing technologies for locally-tailored hybrid composites, suitable for industrial large-scale use, as well as on exploiting the finite element model to identify solutions with even larger synergetic effects.

# 7 Acknowledgements

This project has received funding from the European Union's Horizon 2020 research and innovation programme under the Marie Skłodowska-Curie grant agreement No 654467. YS acknowledges the support of FWO Flanders for his postdoctoral fellowship. STP acknowledges EPSRC for his "NextGen" fellowship (EP/M002500/1).

# 8 References

[1] Laffan MJ, Pinho ST, Robinson P, McMillan AJ. Translaminar fracture toughness testing of composites: A review. Polymer Testing. 2012;31(3):481-489.
[2] Swolfs Y, Verpoest I, Gorbatikh L. Recent advances in fibre-hybrid composites: materials selection, opportunities and applications. International Materials Reviews. 2019;64(4):181-215.

[3] Bullegas G, Pinho ST, Pimenta S. Engineering the translaminar fracture behaviour of thin-ply composites. Compos Sci Technol. 2016.
[4] Pimenta S, Pinho ST. An analytical model for the translaminar fracture toughness of fibre composites with stochastic quasi-fractal fracture surfaces. J Mech Phys Solids. 2014;66(0):78-102.
[5] Catalanotti G, Arteiro A, Hayati M, Camanho PP. Determination of the mode I crack resistance curve of polymer composites using the size-effect law. Engineering Fracture Mechanics. 2014;118:49-65.
[6] Ortega A, Maimí P, González EV, Sainz de Aja JR, de la Escalera FM, Cruz P. Translaminar fracture toughness of interply hybrid laminates under tensile and compressive loads. Compos Sci Technol. 2017;143:1-12.
[7] Teixeira RF, Pinho ST, Robinson P. Thickness-dependence of the translaminar fracture toughness: Experimental study using thin-ply composites. Composites Part A. 2016;90:33-44.
[8] Davies P, Blackman BRK, Brunner AJ. Standard Test Methods for Delamination Resistance of Composite Materials: Current Status. Applied Composite Materials. 1998;5(6):345-364.
[9] Frossard G, Cugnoni J, Gmür T, Botsis J. Mode I interlaminar fracture of carbon epoxy laminates: Effects of ply thickness. Composites Part A. 2016;91:1-8.
[10] Canal LP, Pappas G, Botsis J. Large scale fiber bridging in mode I intralaminar fracture. An embedded cell approach. Compos Sci Technol. 2016;126:52-59.
[11] Czél G, Rev T, Jalalvand M, Fotouhi M, Longana ML, Nixon-Pearson OJ, et al. Pseudo-ductility and reduced notch sensitivity in multi-directional all-carbon/epoxy thin-ply hybrid composites. Composites Part A. 2018;104:151-164.
[12] Ritchie RO. The conflicts between strength and toughness. Nat Mater. 2011;10(11):817-822.
[13] Wegst UGK, Bai H, Saiz E, Tomsia AP, Ritchie RO. Bioinspired structural materials. Nature Materials. 2015;14(1):23-36.
[14] Malkin R, Yasaee M, Trask RS, Bond IP. Bio-inspired laminate design exhibiting pseudo-ductile (graceful) failure during flexural loading. Composites Part A. 2013;54(0):107-116.
[15] Narducci F, Pinho ST. Exploiting nacre-inspired crack deflection mechanisms in CFRP via micro-structural design. Compos Sci Technol. 2017;153:178-189.
[16] Kolednik O, Predan J, Fischer FD, Fratzl P. Bioinspired Design Criteria for Damage-Resistant Materials with Periodically Varying Microstructure. Advanced Functional Materials. 2011;21(19):3634-3641.
[17] Fratzl P, Kolednik O, Fischer FD, Dean MN. The mechanics of tessellations – bioinspired strategies for fracture resistance. Chemical Society Reviews. 2016;45(2):252-267.
[18] Kolednik O, Zechner J, Predan J. Improvement of fatigue life by compliant and soft interlayers. Scripta Materialia. 2016;113:1-5.
[19] Sistaninia M, Kolednik O. Improving strength and toughness of materials by utilizing spatial variations of the yield stress. Acta Materialia. 2017;122:207-219.
[20] Swolfs Y, Gorbatikh L, Verpoest I. Fibre hybridisation in polymer composites: a review. Composites Part A. 2014;67:181-200.
[21] McBride A, Turek S, Zaghi A, Burke K. Mechanical Behavior of Hybrid Glass/Steel Fiber Reinforced Epoxy Composites. Polymers. 2017;9(4):151.
[22] Swolfs Y, Geboes Y, Gorbatikh L, Pinho ST. The importance of translaminar fracture toughness for the penetration impact behaviour of woven carbon/glass hybrid composites. Composites Part A. 2017;103:1-8.

[23] Huang SL, Hess TE. A hybrid composite fuselage design with integral crack arresters. Third conference on fibrous composites in flight vehicle design, Williamsburg, USA: NASA TM X-3377; 1976.
[24] Poe CC, Kennedy JM. An Assessment of Buffer Strips for Improving Damage Tolerance of Composite Laminates. J Compos Mater. 1980;14(1):57-70.
[25] Dilligan MA, Kedward KT. Modeling and assessment of integral crack arrest zones in CFRP laminates. 2007.
[26] Parandoush P, Lin D. A review on additive manufacturing of polymer-fiber composites. Compos Struct. 2017;182:36-53.
[27] Panesar A, Ashcroft I, Brackett D, Wildman R, Hague R. Design framework for multifunctional additive manufacturing: Coupled optimization strategy for structures with embedded functional systems. Additive Manufacturing. 2017;16:98-106.
[28] Wang X, Jiang M, Zhou Z, Gou J, Hui D. 3D printing of polymer matrix composites: A review and prospective. Composites Part B. 2017;110:442-458.
[29] Blanco N, Trias D, Pinho ST, Robinson P. Intralaminar fracture toughness characterisation of woven composite laminates. Part I: Design and analysis of a compact tension (CT) specimen. Engineering Fracture Mechanics. 2014;131:349-360.
[30] Laffan MJ, Pinho ST, Robinson P, McMillan AJ. Translaminar fracture toughness: The critical notch tip radius of 0° plies in CFRP. Compos Sci Technol. 2011;72(1):97-102.
[31] Swolfs Y, Gorbatikh L, Romanov V, Orlova S, Lomov SV, Verpoest I. Stress concentrations in an impregnated fibre bundle with random fibre packing. Compos Sci Technol. 2013;74:113-120.
[32] Chamis CC. Simplified Composite Micromechanics Equations for Hygral, Thermal and Mechanical Properties. NASA Technical Memorandum 88320, Houston, United States: NASA; 1983.
[33] Rizvi GM, Bellehumeur CT, Gu P, Sun Q. Effect of processing conditions on the bonding quality of FDM polymer filaments. Rapid Prototyping Journal. 2008;14(2):72-80.
[34] Laureto JJ, Pearce JM. Anisotropic mechanical property variance between ASTM D638-14 type i and type iv fused filament fabricated specimens. Polymer Testing. 2018;68:294-301.
[35] Blanco N, Trias D, Pinho ST, Robinson P. Intralaminar fracture toughness characterisation of woven composite laminates. Part II: Experimental characterisation. Engineering Fracture Mechanics. 2014;131:361-370.